

Research on Comprehensive Corrosion Behavior of Copper-Nickel Alloys in Multi-Medium Environment

Zhang Yu-Fu^{1,2a*}, Hao Yuan^{1b}, Ma Ying^{1b}, Song Weng-Ming^{1,2c}

*School of Material Science and Engineering, Lanzhou University of Technology,
Postal Code 730050, Lanzhou, China*

Corresponding author is Zhang Yu-Fu

Abstract

In this paper, we studied on the corrosion behavior of copper-nickel alloys in multi-medium environment with different temperature, pressure, and pH value. Referring to the domestic and international standards, we established a new corrosion model of copper-nickel alloys, and measured as well as analyzed influences on the corrosion rate, the corrosion products, the corrosion mechanism caused by the corrosion medium, such as H₂S, CO₂, Cl⁻. The results showed that, the corrosion behavior were different in different environment; while different corrosion medium militated the alloys in the same environment, where we found coupling corrosion behavior. We took the copper-nickel alloys B30, used as the pressure equipment material, in the model experiment under the actual project condition, which would supported the standards revision of materials and material selection in corrosion environment with rich experimental data.

Keywords: COMPREHENSIVE CORROSION, COPPER-NICKEL ALLOYS, CORROSION MEDIUM H₂S, CO₂, CL⁻, CORROSION MECHANISM, COUPLING CORROSION BEHAVIOR

1. Introduction

The research on the material corrosion were mainly conducted at the influences of H₂S, CO₂, Cl⁻ and other corrosion mediums to the materials [1-8]. The film appearances of carbon steel corroded in CO₂/H₂S environment at room temperature and environment temperature were described, and the reasons were analysed [2]. Hydrogen sulfide corrosion of welds in acidic chloride solution was studied as an example of corrosion behavior in multi-medium environment [3]. The curves of corrosion rate and corrosion products were drawn on hydrogen sulfide corrosion in CO₂ acid solution [5]. The fundamental reason that stainless steels (such as 304L and 316L) were corroded in the acid medium was chemical element, which was

proposed by comparing the corrosion situations of these materials [6].

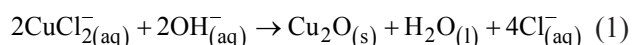
In recent years, the fatigue and failure of the materials caused by the corrosion has been a major area in corrosion research [7-8]. The corrosion behavior of materials with initial defects was studied, and relevant protective measures were proposed [9-13]. Theoretical work on hydrogen sulfide corrosion in materials was conducted by coupling model of phase and polarization behavior [14].

But the survey showed that, the research on the corrosion behavior of copper-nickel alloys in H₂S, CO₂, Cl⁻ and other corrosion mediums with different temperature, pressure, and pH value and interrelationship of them was not conducted, and the material

comprehensive corrosion was caused actually by the factors of above. Therefore, we selected the copper-nickel alloys B30, used as the pressure equipment material, in the model experiment under the actual project condition, and provided a large number of experimental data and curves in this paper.

2. The Corrosion Process Model and the Mechanism Analyses of Copper-Nickel Alloys

Figure 2.1 shows the corrosion process of B30 copper-nickel alloys in multi-medium environment without H₂S. In the initial time of corrosion, the sample surface adsorbs ion formed by the hydrolysis of Cl⁻, SO₄²⁻ and CO₂, and the chloride is formed, where the cationic copper-iron and nickel-ion are discharged and Cl⁻ is the most active iron. Cu is more stable than Ni in thermodynamic and the chloride soluble in water, while monovalence copper ion is increasing on the sample surface, which will form porous film of cuprous chloride and converts into dense film of cuprous oxide, called passive film of copper-nickel. The corrosion process can be expressed as



The cuprous oxide will partially convert into copper oxide as the reaction proceeding. Copper-Nickel alloys would be decoppered or denickeled in the corrosion process, which mainly depends on the electric potential and pH value, and denickelification happens on the sample surface in the acid solution, where the dense film would form and corrosion rate would reduce for dense of maintain current reducing (Qun-Jie Xu, Mao-Rong Ding, Zi-Chao Chen, Huan Chen, 2006; Rong-Jun Zhang, Tian-Ming Zhang, 2007).

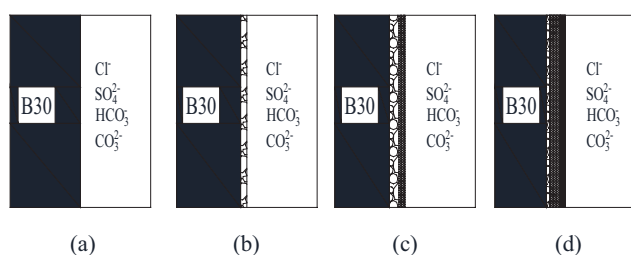
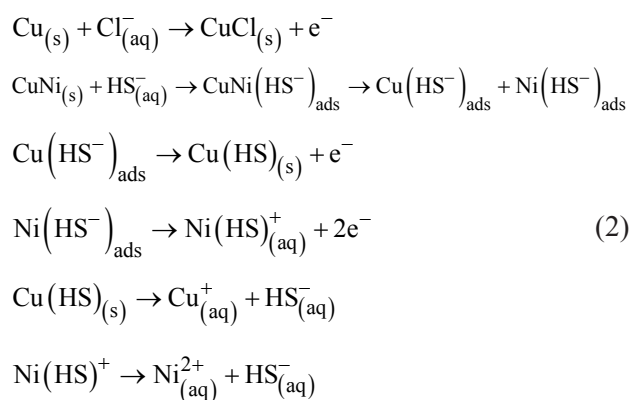


Figure 2.1. The corrosion process model of B30 copper-nickel alloys in multi-medium environment (without H₂S) (a)The initial time of corrosion (b)The formation of CuCl with loose surface (c)The formation of dense Cu₂O on the sample surface (d)The final formation of corrosion product film which contained three layers

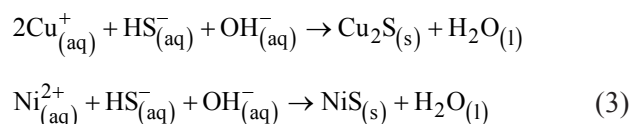
3. The Model Experiment and the Corrosion Rate Analyses of Copper-Nickel Alloys

We took B30 copper-nickel alloys as the corrosion sample, which is used as the pressure equipment material, and prepared 4 kinds of corrosion medium

Figure 2.2 shows the corrosion process of copper-nickel alloys B30 in multi-medium environment with H₂S. In this condition, the sample surface will also adsorb ion formed by the hydrolysis of S²⁻ and HS⁻, and the corrosion process can be expressed as



The following reactions will happen besides (1) when the corrosion process proceeding



At this time, the corrosion products on the loose layer of the sample surface are cuprous chloride, copper sulfide and nickel sulfide. Cuprous chloride will convert into copper oxide and copper sulfide will convert into copper sulfide when the corrosion process proceeding, called the toxic effect of sulfur ion. The corrosion rate will substantially increase for this effect on extinguishing deactivation compared with that without H₂S.

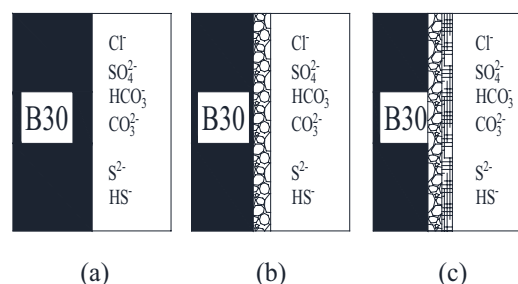


Figure 2.2. The corrosion process model of copper-nickel alloys B30 in multi-medium environment (with H₂S) (a)The initial time of corrosion (b)The formation of loose complex product on the sample surface (c)The formation of dense Cu₂O on the sample surface (d)The final formation of corrosion product film which contained two layers

according to the actual project condition, the components of which are showed in Tab.3.1. The corrosion rate curves of the sample in different corrosion mediums are showed in Figure 3.1.

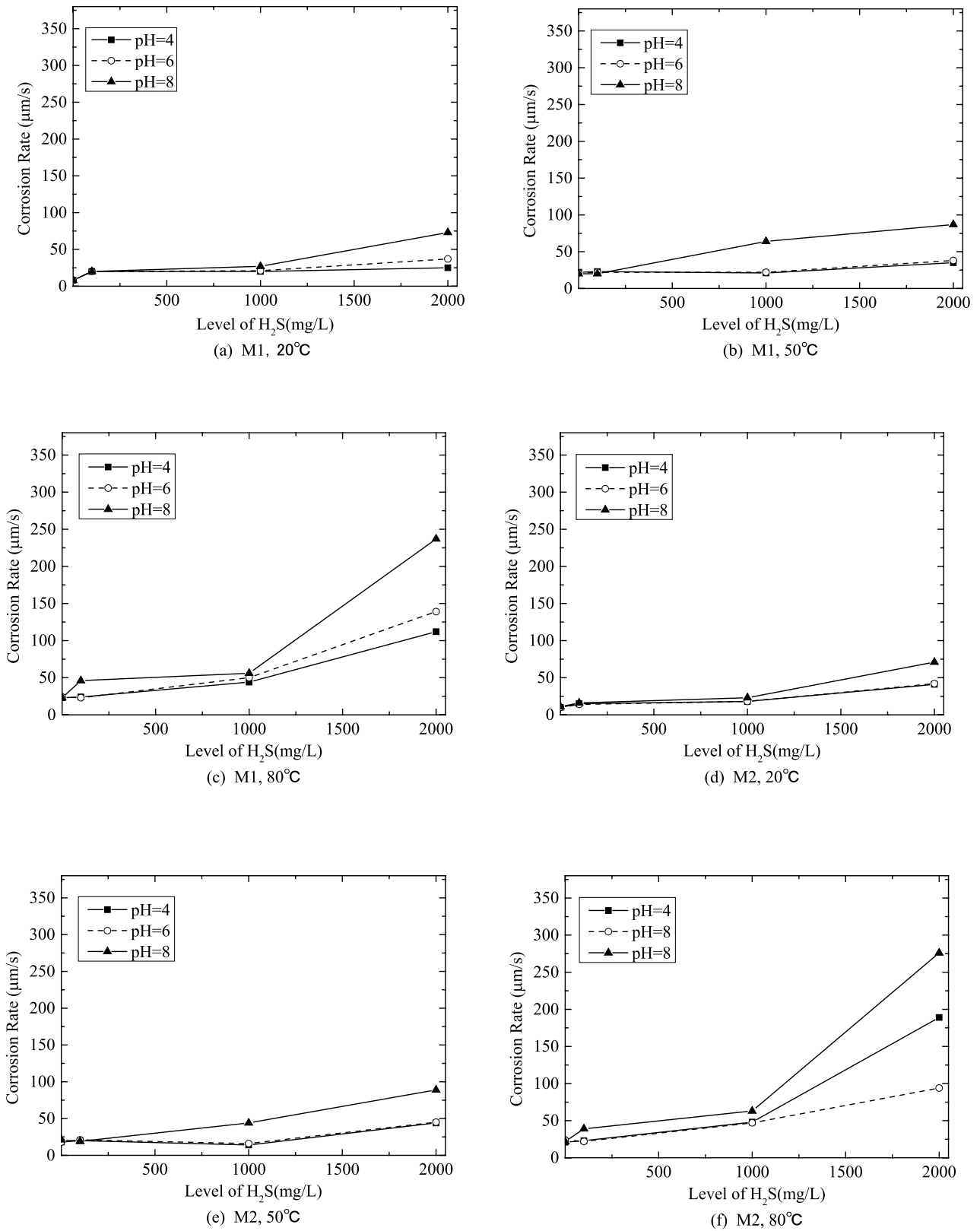
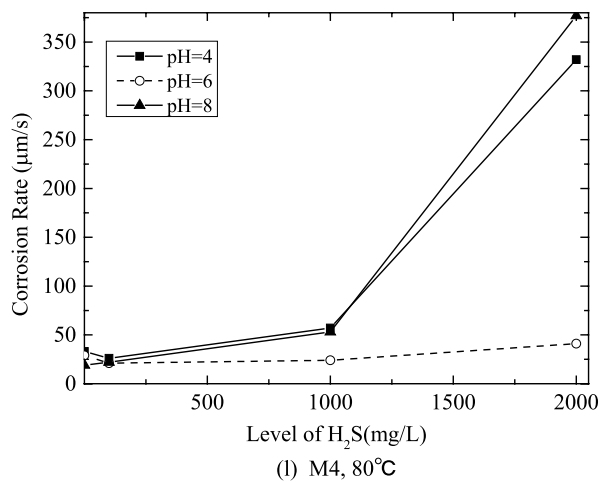
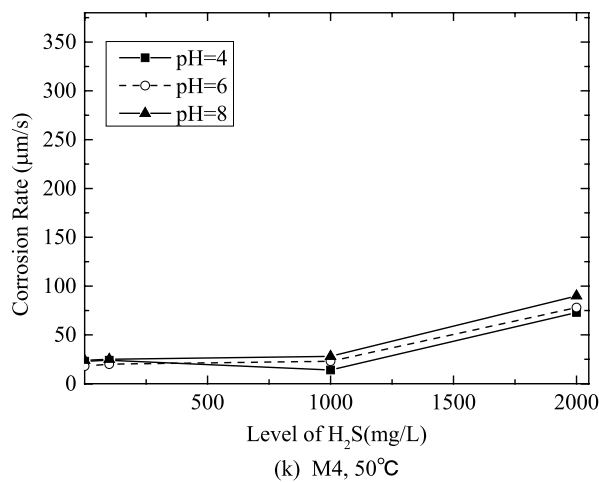
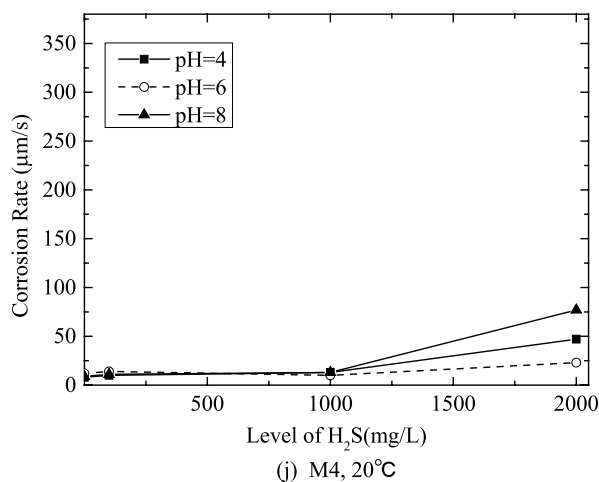
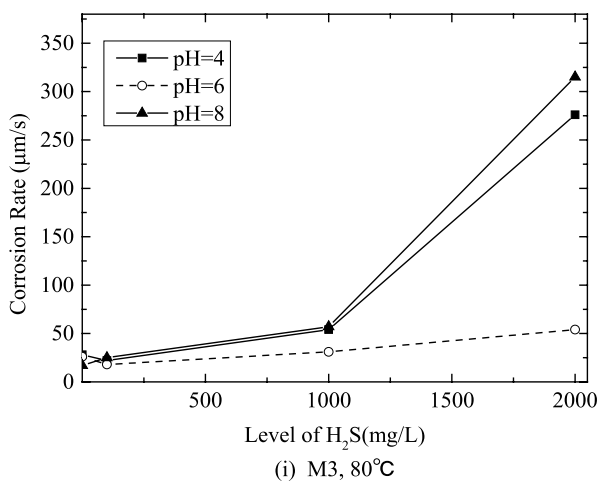
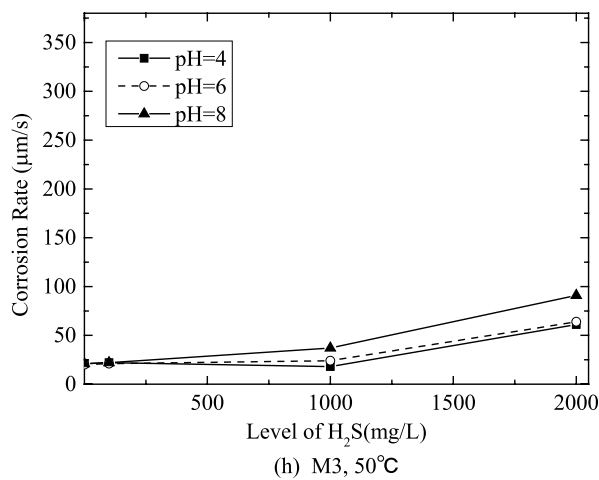
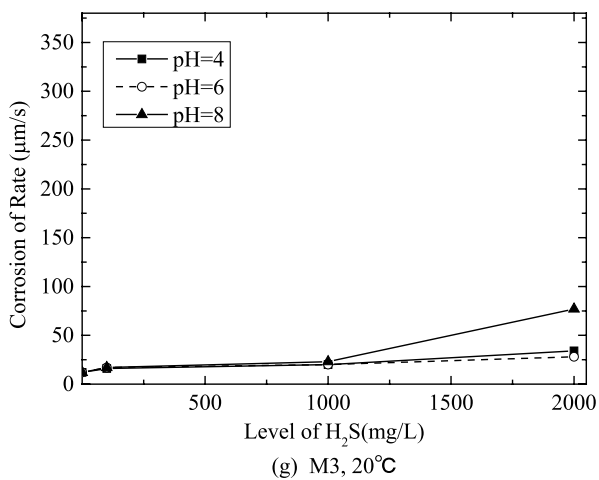


Figure 3.1. The corrosion rates changing along with the content of H_2S , pH



value and temperature in the four different kinds of corrosion solution

Table 3.1. The Test Mediums and Other Components

Components	M1	M2	M3	M4
$\text{Cl}^- / \times 10^3 \text{mg} \cdot \text{L}^{-1}$	170	100	57	1
$\text{F}^- / \text{mg} \cdot \text{L}^{-1}$	40	40	0	0
Na^+	Allowance			
$\text{P}_{\text{CO}_2} / \text{MPa}$	5.0	2	2	1

The model experiment is conducted in the 4 kinds of corrosion solutions showed in Tab.3.1, which are different in the level of hydrogen sulfide. The experiment and analyses of the corrosion rate are on the basis of the second section. The pitting corrosion test of B30 copper-nickel alloys indicates that, the corrosion rate is faster than nickel-base alloy and duplex stainless steel but slower than lean alloy steel. The slow strain rate test of B30 copper-nickel alloys indicates that, the stress sensitivity index increases greatly as the temperature increasing from room temperature to 50°C, while it increases not so fast when the temperature increasing from 50°C to 80°C. The stress sensitivity index of pH=6 is slightly lower than these of pH=4 and pH=8 when temperature is 50°C, but the whole range of this index is less than 25%, so the stress sensitivity of B30 is not obvious.

The variation of corrosion rate of B30 copper-nickel alloys in different corrosion solution with different levels of H_2S , pH value and temperature is summarized and listed as following

The corrosion rate increase along with the increase of the H_2S level in the same solution with the same temperature and pH value, and the corrosion rate curves turn upward when the H_2S level is above 1000mg/L.

The corrosion rate increase along with the increase of the temperature in the same solution with the same H_2S level and pH value, and the maximum increase amount turns up at 80°C.

The corrosion rate increase along with the increase of the pH value in the same solution with the same temperature and H_2S level. In addition, the corrosion rate curves nearly overlap with each when pH=4 and pH=6. Only when the temperature is 80°C and the solution contains H_2S , the corrosion rate curves of pH=4 and pH=8 will be significantly higher than that of pH=6.

Furthermore, the chloride ion concentration and CO_2 partial pressure are different in different solutions, and the corrosion rate increase along with the reduce of the chloride ion concentration and CO_2 partial pressure. Take (c) and (l) for example, the corrosion rate in M4 is nearly 150 $\mu\text{m/s}$ more than that in M1 (more than about 70%). The hydrolysis ions

of Cl^- and CO_2 coexist with hydrogen sulfide, and HS^- , S^{2-} , HCO_3^- , CO_3^{2-} and other ions will emerge, in which Cl^- will be adsorbed on the sample surface and the toxic effect of sulfur ion will be eased by the surge of ion species.

4. Corrosion Morphology and Corrosion Products Analyses of Copper-Nickel Alloys

Figure 4.1 shows the macro morphology of B30 after comprehensive corrosion in M1 and M4. The sample surface is rust red in (a) when pH=8 and temperature is 80°C without H_2S , inferring the possible components are cuprous oxide (dark red or bright red) and copper oxide (black). The sample surface is grey black when pH=8 and temperature is 80°C with H_2S level is 2000mg/L, inferring the possible components are copper sulfide (black) and copper oxide (black).



Figure 4.1. The macro morphology of B30 after comprehensive corrosion (a)contained no H_2S (b)contained $\text{H}_2\text{S}=2000\text{mg/L}$

Figure 4.2 shows the microstructure of B30 after comprehensive corrosion in M4 when H_2S level is 2000mg/L, pH=4, temperature are 20°C, 50°C, 80°C respectively. (a) shows that pits like honeycomb distribute in the corrosion product layer on the sample surface. (b) shows that the size of these pits increases and the corrosion products fall off partly. (c) shows that the shedding is very obvious and the adhesive rate goes down further than that in (b).

Figure 4.3 shows the element analyses of corrosion products on the sample surface in M4 when H_2S level is 2000mg/L and pH=4, which are Cu, S, O and a bit of Ni. The corrosion products contain oxide of Cu and sulfide of Cu. The main corrosion product is cuprous oxide in seawater or solution with chlorine ion, which is red or dark red and insoluble in water. But porous product layer of copper sulfide is easy to form when sulfur ion exist by the obvious toxic effect of it. The molar volume of copper sulfide is 28.4 cm^3 and the molar volume of cuprous oxide is 23.9 cm^3 , so the strain makes the shedding of the corrosion product layer more serious in the conversion process from cuprous to copper sulfide with the increase of the reaction time and temperature.

Figure 4.4 shows XPS atlas of corrosion products on the sample surface in M1 and M4. The corrosion products curve of M1 is above that of M4, and they

all contain Cl2p, O1s, Cu2p, Ni2p. However, the Cl2p peak signal and Ni2p peak signal of M4 are relatively strong than that of M1, and S2p peak signal of M4 emerges.

Figure 4.5 (a) (b) show the XPS atlas of Cu in the corrosion products on the sample surface respectively in M1 and M4. (a) shows that the bending energy of Cu2p3/2 of M1 is between 926eV and 936eV, and the relative intensities got from the fitting curve are 930.8eV, 932.5eV and 933.6eV, which are correspond to CuCl, Cu₂O/Cu, CuO respectively. So it can be calculated that the components of corrosion products are 9%CuCl, 63%Cu₂O/Cu and 28%CuO (V. Garcia-Arriaga, J. Alvarez-Ramirez, M. Amaya, E. Sosa, 2010; J. Amri, T. Souier, B. Malki, B. Baroux, 2008; C.D. Wagner, J.F. Moulder, L.E. Davis, W.M. Riggs, 1992), and the dense corrosion product layer on the sample surface is mainly cuprous oxide (J. Amri, T. Souier, B. Malki, B. Baroux, 2008). Besides, Cu₂(OH)₃Cl is not found in the corrosion products layer because of the corrosion time is not enough probably. (b) shows that the bending energy of Cu2p3/2 of M4 is also between 926eV and 936eV, and the relative intensities got from the fitting curve are 930.8eV, 932.5eV and 933.8eV, which are correspond to CuCl, Mixture of Cu/Cu₂S/Cu₂O (which are difficult to distinguish with each other for the bending energy differ no more than 0.1eV), CuO respectively. So it can be calculated that the components of corrosion products are 32.5%CuCl, 53.4%Cu/Cu₂S/Cu₂O and 14.1%CuO (G. Kear, B.D. Barker, K. Stokes, F.C. Walsh, J. Appl, 2004; H. Jang, H. Kwon, 2006; C.D. Wagner, J.F. Moulder, L.E. Davis, W.M. Riggs, 1992), and the level of cuprous chloride increased in the corrosion products on the sample surface in the solution with H₂S.

Porous corrosion product layer of cuprous chloride is ordinarily regarded as the first generation on the copper-nickel alloys corroded in the chloride ion medium environment (G. Kear, B.D. Barker, K. Stokes, F.C. Walsh, J. Appl, 2004; H. Jang, H. Kwon, 2006). The level increase of CuCl and the level decrease of Cu₂O indicate that the corrosion reaction is continuous on the sample surface in the solution with H₂S, leaving a loose and porous layer by destroying the dense oxide film, refer to Figure 4.2. The level increase of CuCl is the specific example of toxic effect of sulfur ion.

Figure 4.6 (a) (b) show the XPS atlas of Ni in the corrosion products on the sample surface respectively in M1 and M4. (a) shows that level of Ni is very low, which are mainly NiO and Ni(OH)₂. (b) shows that nickel sulfide is the mainly corrosion product,

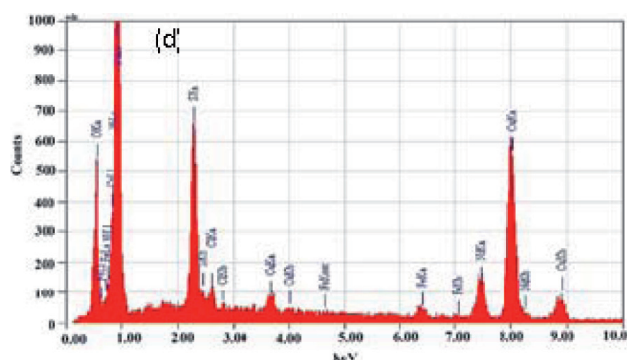


Figure 4.3. The element analyses of corrosion products on the sample surface

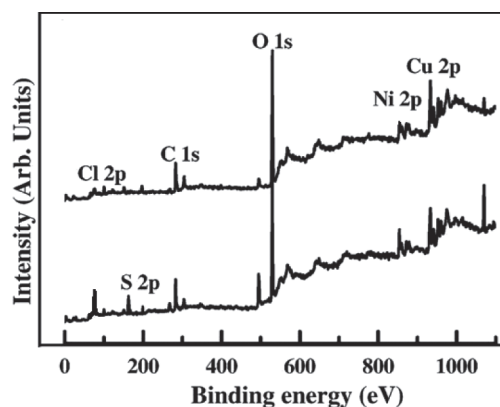


Figure 4.4. XPS atlas of corrosion products on the sample surface

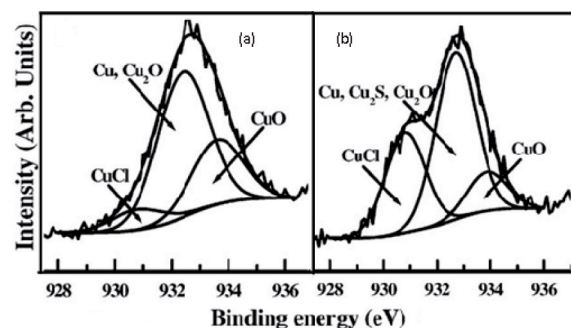


Figure 4.5. XPS atlas of Cu in the corrosion products on the sample surface (a) contained no H₂S (b) contained H₂S=2000mg/L

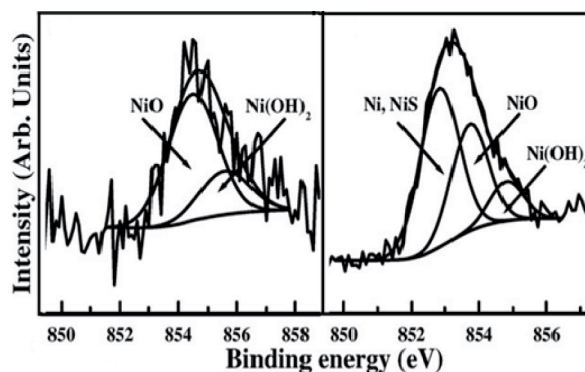
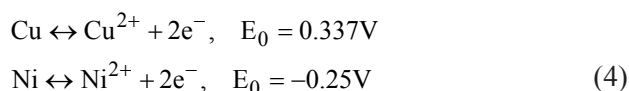


Figure 4.6. XPS atlas of Ni in the corrosion product on the sample surface (a) contained no H₂S (b) contained H₂S=2000mg/L

and the relative intensities got from the fitting curve are 852.8eV, 853.6eV and 855.2eV, which are correspond to Ni/NiS, NiO, Ni(OH) respectively.

The corrosion product layer of copper-nickel alloys is ordinarily composed with 2 layers in seawater, which is mainly CuO and Cu(OH)₂ of the outer layer and Cu₂O mingle with Ni or Fe of the inner layer. There may be a third one in the internal layer and could not display in the atlas, which is extremely thin and porous CuCl layer coverer by the 2 dense layers outside (M.P. Seah, 2005; V. Garcia-Arriaga, J. Alvarez-Ramirez, M. Amaya, E. Sosa, 2010). As a result of the porous outer layers in the solution with H₂S, CuCl is able to display in the atlas.

According to the corrosion thermodynamics (Véronique Smanio, Marion Fregonese, Jean Kittel, 2011), the HCR of Cu and Ni are as follow



Therefore, Ni is more easily dissolved than Cu in open circuit, and dense protective layer is formed on the sample surface in oxidizing atmosphere condition, where the oxide of copper is generated with increase level of copper and the oxide of nickel is mixed in. Figure 4.7 shows the XPS atlas of S in the corrosion products on the sample surface respectively in M1 and M4. The XPS curve of S of M4 is above that of M1, but S2p signal is relatively strong. The fitted peak spectrum of M1 is about 168eV corresponding to SO₄²⁻, and the fitted peak spectrum of M4 are about 161.6eV and 162.8eV corresponding to 70%Cu₂S and 30%NiS/CuS respectively, so the sulfide of corrosion product is mainly Cu₂S.

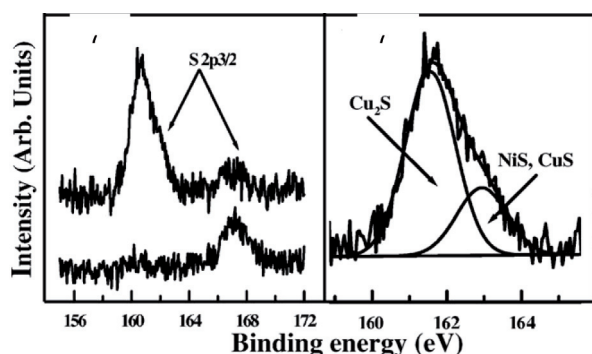


Figure 4.7. XPS atlas of Ni in the corrosion product on the sample surface
(a)contrast between M1 and M4 (b)contained H₂S=2000mg/L

5. Conclusions

The corrosion rate of B30 copper-nickel alloys is low in the solution with hydrogen sulfide because of the dense oxide layer on the sample surface. On the

contrary, the corrosion rate aggravates along with the H₂S level, pH value and temperature in the solution with hydrogen sulfide because the sample surface is porous.

The polarization behavior curves of B30 copper-nickel alloys in different corrosion mediums indicate that, the toxic effect of sulfur ion will be eased by the raise of the chloride ion concentration and CO₂ partial pressure when the H₂S partial pressure remains unchanged.

The pitting corrosion test of B30 copper-nickel alloys indicates that, the corrosion rate increases rapidly along with the raise of temperature, which is faster than nickel-base alloy and duplex stainless steel but slower than lean alloy steel.

The microstructure of B30 copper-nickel alloys shows that, the center part of the corrosion pits is not corroded, the main components of which are Cu and a bit of O and S, therefore, pitting begins from the grain boundary or on the interface of α -phase and matrix.

The slow strain rate test of B30 copper-nickel alloys indicates that, the whole range of the stress sensitivity index is less than 25%, so the stress sensitivity of B30 is not obvious.

Acknowledgments

This work was supported by the Science and Technology Support Program of Lanzhou City with Grant NO.20090113.

References

1. B.F.M. Pots, R.C. John, et al. Improvement on De Waard-Milliams corrosion prediction and application to corrosion management, NACE Corrosion, 2002, No.02:235.
2. J. Kvarekval, R. Nyborg, M. Seiersten, Corrosion product film on carbon steel in semi-sour CO₂/H₂S environment, NACE Corrosion, 2002, No.02:296.
3. L.W. Tsay, Y.J. Lin a, C. Chen, The effects of rolling temperature and sensitization treatment on the sulfide stress corrosion cracking of 304L stainless steel, Corrosion Science, 2012,63:267-274.
4. Fragieli, S. Serna, R. Pérez, Electrochemical study of two microalloyed pipeline steels in H₂S environments, International Journal of Hydrogen Energy, 2005, 30:1303-1309.
5. E. Abelev, J. Sellberg, T. A. Ramanarayanan, Effect of H₂S on Fe corrosion in CO₂ - saturated brine, J. Mater. Sci. 2009, 44:6167-6181.
6. Davoodi, M. Pakshir, M. Babaiee, G.R. Ebrahimi, A comparative H₂S corrosion study of

- 304L and 316L stainless steels in acidic media, *Corrosion Science*, 2011, 53:399-408.
- Pfennig, R. Wiegand, M. Wolf, C.-P. Bork, Corrosion and corrosion fatigue of AISI 420C (X46Cr13) at 60°C in CO₂-saturated artificial geothermal brine, *Corrosion Science*, 2013, 68:134-143.
 - J. Kittel, F. Ropital, F. Grosjean, E.M.M. Sutter, B. Tribollet, Corrosion mechanisms in aqueous solutions containing dissolved H₂S. Part 1: Characterisation of H₂S reduction on a 316L rotating disc electrode, *Corrosion Science*, 2013, 66:324-329.
 - Z. F. Yin, L. Liu, Y. Q. Zhang, K. Wang, Characteristics and mechanism of corrosion film formation on antislulphur steels in CO₂/H₂S environments, *Corrosion Engineering, Science and Technology*, 2012, 47(2):138-146.
 - E.G. Webb, R.C. Alkire, Pit Initiation at single sulfide inclusions in stainless steel III. Mathematical model, *Journal of the Electrochemical Society* 149 (2002):B286-B295.
 - R. Avci, B.H. Davis, M.L. Wolfenden, Mechanism of MnS-mediated pit initiation and propagation in carbon steel in an anaerobic sulfidogenic media, *Corrosion Science* 76 (2013):267-274.
 - G. Hinds, L. Wickstr, K. Mingard, A. Turnbull, Impact of surface condition on sulphide stress corrosion cracking of 316L stainless steel, *Corrosion Science*, 2013, 71:43-52.
 - P. Marcus, V. Maurice, H.H. Strehblow, Localized corrosion (pitting): a model of passivity breakdown including the role of the oxide layer nanostructure, *Corrosion Science*, 2008, 50:2698-2704.
 - E. Abelev, J. Sellberg, T. A. Ramanarayanan, Effect of H₂S on Fe corrosion in CO₂-saturated brine, *J Mater Sci*, 2009, 44:6167-6181.
 - Qun-Jie Xu, Mao-Rong Ding, Zi-Chao Chen, Huan Chen, Influence of Tin and Zinc on Corrosion Resistance of Copper Alloys, *Journal of Shanghai University of Electric Power*, 2006, 22(3):229-233.
 - Rong-Jun Zhang, Tian-Ming Zhang, Electrochemical Studies of Inhibition Effects for B30 Cu-Ni Alloy Corrosion in Simulated Water. *Corrosion & Protection*, 2007, 28(2):65-68.
 - V. Garcia-Arriaga, J. Alvarez-Ramirez, M. Amaya, E. Sosa, H₂S and O₂ influence on the corrosion of carbon steel immersed in a solution containing 3 M diethanolamine, *Corrosion Science* 52 (2010) :2268-2279.
 - J. Amri, T. Souier, B. Malki, B. Baroux, Effect of the final annealing of cold rolled stainless steels sheets on the electronic properties and pit nucleation resistance of passive films, *Corrosion Science*, 2008, 50:431-435.
 - C.D. Wagner, J.F. Moulder, L.E. Davis, W.M. Riggs, *Handbook of X-ray Photoelectron Spectroscopy*, Perkin-Elmer Corp., Physical Electronics Division, Minnesota, 1992.
 - G. Kear, B.D. Barker, K. Stokes, F.C. Walsh, *J. Appl. Electrochem.* 34 (2004) :659-669.
 - H. Jang, H. Kwon, In situ study on the effects of Ni and Mo on the passive film formed on Fe-20Cr alloys by photoelectrochemical and Mott-Schottky techniques, *Journal of Electroanalytical Chemistry*, 2006, 590:120-125.
 - M.P. Seah, Ultrathin SiO₂ on Si. VI. Evaluation of uncertainties in thickness measurement using XPS, *Surface and Interface Analysis*, 2005, 37:300-309.
 - V. Garcia-Arriaga, J. Alvarez-Ramirez, M. Amaya, E. Sosa, H₂S and O₂ influence on the corrosion of carbon steel immersed in a solution containing 3 M diethanolamine, *Corrosion Science* 52 (2010) :2268-2279.
 - Véronique Smanio, Marion Fregonese, Jean Kittel, Contribution of acoustic emission to the understanding of sulfide stress cracking of low alloy steels, *Corrosion Science* 53 (2011) :3942-3949.

Metallurgical and Mining
Industry

www.metaljournal.com.ua